JOURNAL OF MATERIALS SCIENCE **36** (2001) 2257–2270

Rate effects on the delamination fracture of multidirectional carbon-fiber/epoxy composites under mode I loading

N. S. CHOI
Department of Mechanical Engineering, Hanyang University, Ansan-si, Kyunggi-di, 425-791, Korea
E-mail: nschoi@email.hanyang.ac.kr

The present study has shown the experimental results for characterization of the mode I delamination fracture of continuous carbon fiber/epoxy multidirectional composites under a wide range of test rates, up to high rates of 11.4 m/s. At the slow rates of test $\leq 1.0 \times 10^{-1}$ m/s the delamination fracture energy showed a rising "R-curve", a strong function of the length of propagating crack due to the large extent of crack jumping and following fiber bridging. At the high rates of test ≥ 1.0 m/s any loads recorded by the load cell were largely obscured by such dynamic effects as "spring-mass" oscillations and flexural wave reflections. In this respect, Equation 11, requiring the values of the actual arm displacement and flexural (axial) modulus, was better for the deduction of G_{IC}. However the maximum value of G_{IC} so obtained was considerably underestimated. By increasing the rate up to 1.0×10^{-1} m/s, there were little differences in the delamination fracture behaviors, whereas at high rates > 1.0 m/s the maximum values of G_{IC} decreased considerably. In the case of a short initial crack length, however, the maximum values largely increased at a rate of 11.4 m/s.

1. Introduction

Fiber composites, based on continuous fibers embedded in a polymeric matrix, are very promising for applications in various mechanical structures where a high stiffness-to-weight ratio and strength-to-weight ratio are required. A limitation of many fiber composites, however, is their poor resistance to delamination. The existence of delaminations will not only lead to a loss of stiffness, but also to a degradation in strength and service-life, which can be a very important consideration in the design and use of laminated fiber composite structures.

The majority of the work on the delamination fracture of composite materials has been conducted through the application of linear-elastic fracture-mechanics (LEFM), which is concerned with the determination of the interlaminar fracture energy Gc [1–21]. Since the propagation of the crack is constrained in the same plane between the laminate irrespective of the applied loads, various modes of fracture, i.e. Mode I (tensile loading), Mode II (in-plane shear) and Mixed-Mode I/II are identified. Among the modes, Mode I fracture shows the lowest Gc values.

The interlaminar fracture energy G_{IC} often shows an initial increase with crack length: an increasing resistance effect, i.e. rising "R-curve" is found during the initial propagation of a crack. The behavior of rising "R-curve" is different depending on the polymer matrices [1, 2], layup angles and geometry [3–15], which mainly arises from the increasing degree of fiber bridging developing behind the crack-tip, crack-tip blunting and/or damage zone developing around the crack-tip.

As fiber composites have been increasingly applied in engineering structures, characterization of the interlaminar fracture behavior under high-rate loading has been significant. For unidirectional fiber composites, several researchers [17, 18] have reported decreasing features of G_C with increasing test rates. The extent of decreasing rate in G_{IC} for similar fiber-composites was considerably varied from report to report. A few other researchers [19] reported an increasing behavior in G_{IC} which conflicted with the former reports. Lately Blackman *et al.* [20] showed that considerable care must be taken in the experimental aspects when undertaking the tests at high rates of test: the displacement of the ram of the test machine and the loads recorded by the load cell do not necessarily reflect the actual displacement and actual load experienced by the specimen, respectively. They suggested a measurement of the displacement and corresponding crack length from high-speed photography for the determination of G_{IC}, which did not require a knowledge of the load showing a violent oscillation with the high-rate test. For the PEEK/carbon-fiber composite only a modest reduction (not exceeding 20% of the static value of G_{IC} at crack initiation) was apparent at ratios in excess of 5 m/s. In the case of the epoxy/carbon-fiber composite, the G_{IC} value remained insensitive to the test rates. They further

analysed the dynamic effects on the behavior of G_{IC} being invariably associated with high-rate tests [21].

The above high-rate test studies were all conducted on unidirectional fiber composites. The purpose of the present study is to characterize the mode I—delamination fracture of continuous carbon fiber/epoxy multidirectional laminates under slow and high rates of test (0.5 mm/min—11.4 m/s). Recently, the present author studied the delamination fracture of the multidirectional laminates under a slow rate of test (0.5 mm/min) [15] and showed that the effective flexural modulus and the interlaminar fracture energy were a strong function of the length of propagating crack due to the large extent of crack jumping and ensuing fiber bridging. The values of G_{IC} at crack initiation were significantly greater than those for the corresponding unidirectional laminates. On the basis of the static test results the present study considers (i) the variation of the flexural modulus of the multidirectional laminate with test rates, (ii) the dynamic effects in the double-cantilever beam tests, (iii) the evaluation methods for deduction of G_{IC} in the high-rate tests, (iv) the variation of the propagating crack length and velocity with loading time and, thus, (v) rate effects on the behavior of the delamination fracture energy.

2. Theoretical consideration

2.1. Static analysis

In the standard Mode I double-cantilever beam(DCB) specimen as shown in Fig. 1 with an end deflection of δ, a crack length of a and beam width B, the two arms of the test specimen are loaded by applying symmetrical opening loads. For the static analysis the value of the interlaminar fracture energy G_{IC} is derived in the usual way from [5]

$$G_{IC} = \frac{1}{B}\left(\frac{dU_{ext}}{da} - \frac{dU_s}{da}\right) = \frac{P^2}{2B}\frac{dC}{da} \quad (1)$$

where U_{ext} is the external work, U_s the strain energy, P the end load and C the compliance (δ/P).

From the modified beam theory [5, 6], the expression for the compliance is given by

$$\mathrm{C} = \delta/\mathrm{P} = \frac{8N}{Bh^3E_{11}} \cdot (a + \chi_I h)^3 \quad (2)$$

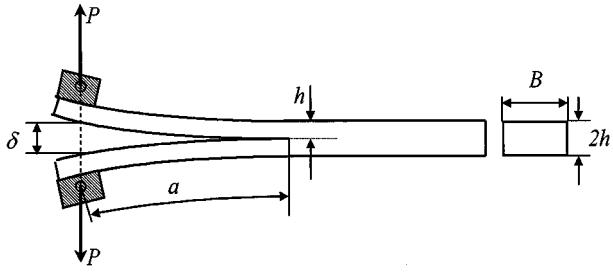

Figure 1 The Mode I double cantilever beam (DCB) composite specimen.

where h is the thickness of one arm of the specimen; E_{11} the axial(flexural) modulus of the laminate arm; χ_I a correction to the crack length to allow for end-rotation and deflection of the crack tip and N a correction for the stiffening caused by the metal end-blocks.

The axial (or flexural) modulus E_{11}, which can be determined from the DCB test, is expressed [5] by

$$E_{11} = \left(\frac{P}{\delta}\right) \cdot \frac{8N(a + \chi_I h)^3}{Bh^3} \quad (3)$$

Differentiating Equation 2 and substituting for P in Equation 1, the Mode I interlaminar fracture energy G_{IC} may be expressed [5, 15] by

$$G_{IC} = \frac{F}{N} \cdot \frac{3P\delta}{2B(a + \chi_I h)} \quad (4)$$

or, alternatively

$$G_{IC} = \frac{F}{N^2} \cdot \frac{3h^3\delta^2 E_{11}}{16(a + \chi_I h)^4} \quad (5)$$

where F is a correction for large displacement.

From Equation 4 the value of G_{IC} can be deduced directly by measuring the crack length a and corresponding values of P and δ. However, a problem that arises with the high-rate tests is that the measured load oscillates violently and an accurate load P cannot be measured. Since Equation 5 does not require a direct knowledge of the load, the expression (5) may be used for deducing values of G_{IC} in the high-rate tests. In this case, the value of the modulus E_{11} in addition to displacement δ has to be determined.

For the DCB fracture tests with an assumption $a = 0$ at $t = 0$, $\delta = Vt$ where V is the test velocity (or displacement rate) and is a constant for each test. Assuming that the material has a constant toughness G_{IC} and the crack propagates in a steady state, the crack length a may be expressed [21] from Equation 5 as

$$a + \chi_I h = At^{1/2} \quad (6)$$

where A is a constant given by

$$A = \left(\frac{3}{16} \cdot \frac{F}{N^2} \cdot \frac{h^3 E_{11} V^2}{G_{IC}}\right)^{1/4} \quad (7)$$

.

2.2. Dynamic effects

For the dynamic analysis of a DCB specimen, the Mode I energy release rate G_{IC} is derived [5] from

$$G_{IC} = \frac{1}{B}\left(\frac{dU_{ext}}{da} - \frac{dU_s}{da} - \frac{dU_k}{da}\right) \quad (8)$$

where U_k is the kinetic energy. Using the "Berry Method" [22, 23], where the static displacement profile is assumed, useful approximations for G_{IC} can be obtained including the kinetic energy term. Two expressions for G_{IC} via Equations 5 and 8 can be derived [21]:

Firstly, prior to crack initiation where crack velocity $\acute{a} = 0$,

$$G_I = \left(\frac{3}{16} \cdot \frac{F}{N^2} \cdot \frac{h^3 E_{11} V^2}{(a + \chi_I h)^4}\right) \cdot t^2 - \frac{33 E_{11} h}{560}\left(\frac{V}{C_l}\right)^2 \tag{9}$$

where C_l is the longitudinal wave speed in the composite arms and is given for the plane strain condition by

$$C_l = \left[\frac{E_{11}}{\rho(1-\nu^2)}\right]^{1/2} \tag{10}$$

where ρ is the specimen density and ν the Poisson's ratio.

Secondly, for steady-state crack propagation when $\acute{a} > 0$, there is a crack velocity contribution to the kinetic energy term. Therefore,

$$G_I = \left(\frac{3}{16} \cdot \frac{F}{N^2} \cdot \frac{h^3 E_{11} V^2}{(a + \chi_I h)^4}\right) \cdot t^2 - \frac{111 E_{11} h}{1120}\left(\frac{V}{C_l}\right)^2 \tag{11}$$

The kinetic energy term in Equation 11 at the high rate of test (11.4 m/s) in this study is predicted to have a value of 2.8×10^{-2} kJ/m^2, which is about 9% of the static energy term at the crack initiation. Since Equation 9 has less kinetic energy term, the crack will initiate at G_I (Equation 9) $= G_{IC}$ which is larger than the value of G_{IC} (Equation 11). There should be a transition region of crack growth before the crack reaches its steady state. When the steady-state propagation is reached, Equation 6 is allowable again, but the value of A is then given by

$$A^4 = \frac{3F \cdot E_{11} h^3 V^2}{16N^2\left(G_{IC} + \frac{111}{1120} E_{11} h\left(\frac{V}{C_l}\right)^2\right)} \tag{12}$$

In the transition region, transient effects will arise leading to more or less non-linear oscillations and perturbations in the crack growth. It is to be further mentioned that effects of stress waves propagating in the specimen are not taken into account in Equations 9 and 11.

3. Experimental

3.1. Multidirectional composite specimens

The multidirectional fiber composite panels were prepared from 24-ply layups of $(-45^\circ/0^\circ/+45^\circ)_{2S}(+45^\circ/0^\circ/-45^\circ)_{2S}$ utilizing a continuous unidirectional carbon fiber/epoxy prepreg tape ('Fibredux 6376C' supplied by Ciba Geigy plc, UK). A layer of "Teflon" release-film 12.5 μm thick was inserted onto the $-45^\circ/+45^\circ$ interface at the mid-plane of the laminate lay-up in order to make the initial delamination (that acts as a starter crack for the interlaminar fracture testing). This thin film was adopted to minimize the formation of a resin-rich region in front of the initial delamination. The composite panels were cured at a temperature of 175°C and a pressure of 0.67 MPa for two hours in an autoclave according to the manufacturer's instructions. The fiber volume fraction and total thickness of the laminate were nominally 65% and 3.4 mm, respectively.

From the cured panels, the specimens were cut to nominally 24.5 mm wide and 130 mm long. The specimen's longitudinal direction was parallel with the direction of the fibers in the 0° ply of the laminates. The thickness and width of each specimen were measured using a micrometer.

One longitudinal edge of the test specimens was coated with a white brittle paint, i.e., type writer correction fluid, to render the crack tip more visible, and was marked with a millimeter scale to aid the measurement of the crack-tip location. Aluminium end-blocks were then adhesively bonded onto each side at the end of the arms of the specimen where the layer of release-film had been placed.

3.2. Mode I interlaminar fracture tests

3.2.1. Slow-rate tests

Slow-rate tests were performed at constant displacement rates of 0.5 mm/min (i.e., 0.83×10^{-5} m/s) and 5 mm/min (i.e. 0.83×10^{-4} m/s) using a screw-driven tensile-testing machine. The tests were conducted at 23 ± 2°C. Three to five replicate specimens were tested for each loading condition. The load versus displacement trace was recorded throughout the test and the corresponding length of the crack was monitored employing a traveling microscope mounted in front of the specimen. These data were also marked on the trace at regular intervals. An accurate value of the initial crack length of each specimen was ascertained by examining the fracture surface after testing of the specimen. Values of the apparent crack length marked on the trace were then corrected by reference to this accurate value for the initial crack length.

3.2.2. High-rate tests

At intermediate and high test rates i.e., in excess of 1.0×10^{-2} m/s and up to 11.4 m/s a servo-hydraulic testing machine (Instron Model 1343) was used. The loading apparatus for the high-rate tests is shown in Fig. 2. The DCB specimens were fixed on to the test rig between two titanium shackles. The upper shackle was fixed to a titanium "lost motion device" [20] which was inserted into the hydraulic ram of the testing machine. Since the stiff nature of the contact area between the device and the ram has a considerable influence on the dynamics of the tests (eg. resulting in "a bouncing effect" [20, 22] and, thus, in a transient loading rate), we reduced the contact stiffness by setting an "aluminium cup and cone" [20] device (inserted with a thin viscoelastic rubber layer between the lost-motion device and the hydraulic ram) so that the lost motion device could make the displacement of the DCB specimen arm smoothly accelerate. Prior to conducting the tests, the position of the lost-motion device was set to allow a period of pre-travel to ensure that the test was conducted at constant velocity. The lower shackle on the stationary

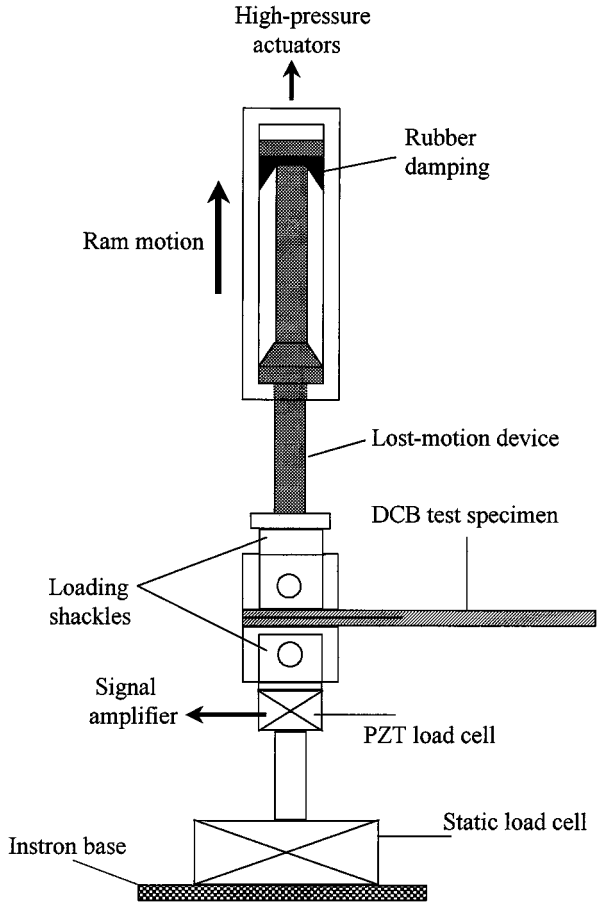

Figure 2 Schematics of loading rigs for the DCB test specimen.

side of the specimen was coupled to the piezo-electric load cell (PCB 208A) having a high natural frequency of 70 kHz and a short rise-time of 10 μs. The tests were performed at $23 \pm 2^{\circ}$C. Three to five replicate specimens were tested for each test-rate condition. Each output signal was amplified and the test data were acquired using a 20 MHz digital oscilloscope (Gould 1600) and a personal computer with a Dadisp signal analysis software. For reference, the oscilloscope also captured the signal of ram displacement versus time from the LVDT transducer mounted on the ram.

Each test was photographed using a high speed camera (Hadland 16 mm Photec IV) with a maximum operation speed of 40,000 frames per second. The optics incorporated a 45 mm, f 2.8 lens, a rotating prism and an associated half-frame image converter. A 16 mm high-speed black and white negative film (KODAK RAR 2479/EASTAR-AH base) was used to provide a high resolution record of the test specimen. A timing-light generator was incorporated into the camera, which marked the film with a 1 kHz time base for a camera speed of greater than 2000 frames per second. To determine the actual specimen displacement δ and the crack length a at any time during the test, each film negative was projected and greatly enlarged onto a screen, from which precise measurement of the crack length and specimen arm displacement could be made. An accurate value of the initial crack length of each specimen was ensured by observing the fracture surface after testing and was used for correction of the apparent crack lengths measured with the high-speed photography.

The oscilloscope and camera were triggered in order to capture the corresponding values of the load, ram displacement, specimen displacement and crack length as a function of time.

3.3. Evaluation of flexural modulus E_{flex}

To deduce values for the Mode I interlaminar fracture energy G_{IC} of the fiber composites via Equations 5, 9 or 11, the value of the flexural modulus E_{flex} should be accurately determined. Thus, a series of three-point bend tests was performed at constant displacement rates of 0.5 mm/min and of up to 11.4 m/s, which corresponded to the test rates used in the interlaminar fracture tests. Bend specimens were the multidirectional composite beams about 1.7 mm in thickness (h), about 11.5 mm in width (b) and 60 mm in test span (S), which was the same fiber composite materials as the ones used in the fracture tests. The thickness and width of each specimen were measured using a micrometer.

In the slow rate test, the screw-driven tester was employed. Values of the E_{flex} were measured from the initial linear elastic region of the load (P)-displacement (δ) curve employing the relation

$$E_{\text{flex}} = \frac{S^3}{4bh^3} \cdot \left(\frac{P}{\delta}\right) \tag{13}$$

In the intermediate and high-rate tests, the servo-hydraulic tester was used. A small V-shaped striker of about 1.5 mm in the tip radius and 3.6 g in weight was made of a light weight and high strength aluminium alloy to minimize the inertia effect caused by the striker mass during the high speed impact testing. The dynamic load to the specimen was measured as a function of time through the PZT load cell installed between the striker and the ram.

Fig. 3a and b shows the load signals measured at test rates of 0.1 m/s and 4.94 m/s, respectively. Components having high frequencies beyond 20 kHz were removed in the load signals. At a test rate of 0.1 m/s, the load exhibited a linearly increasing behavior with increasing time in advance of the brittle fracture at the maximum load point. At test rates lower than 1.0 m/s, values of the flexural modulus were determined through Equation 13 from the slope (P/δ) of the initial linear elastic region. On the other hand, at a test rate of 4.94 m/s, a considerably high amplitude load signal arose in the initial period of impact, which might be related not with specimen deformation behavior but with an inertia effect of the specimen itself. Average values of the dynamic loads showed an increase with time, but was drastically reduced after the fracture. Assuming that one side of a specimen with a half length (S/2) of the total span is perfectly clamped while the other side is pin-clamped, resonant frequency at the first mode in the free flexural vibration is calculated to be 9.7 kHz. This frequency was in a range of the measured ones which increased from 8.4 kHz to 10.2 kHz as the signal cycle proceeded from the second cycle onwards. The reason for the increase in resonant frequency might be that the deformed specimen was stiffer in the loading direction and its

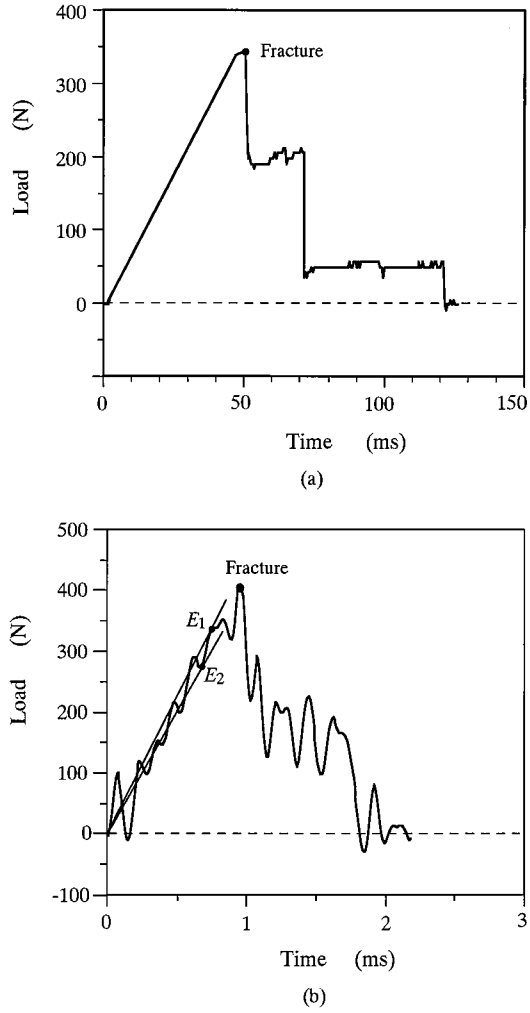

Figure 3 Load-time traces of the multidirectional composites tested at a displacement rate of (a) 0.1 m/s and (b) 4.94 m/s.

geometry was largely changed from the initial state of the specimen at the instant of the impact. However, the measured frequency of the first cycle was about 6.8 kHz, which was considerably lower than the calculated one. At the impact only, the specimen beam is considered to have behaved basically as the free flexural vibration of the specimen with a full span [22].

Suppose that the flexural modulus is not varied with the time of loading. Except for the first cycle formed by an inertia effect, the two consecutive upper and lower peaks in advance of the maximum load in the $P-\delta$ curve are adopted to measure the average value of the corresponding slopes (i.e. $(E_1+E_2)/2$ in Fig. 3b), which is used in the measurement method of E_{flex} through Equation 13 at test rates $\geq$1.0 m/s.

While the axial modulus of unidirectional fiber composites is not significantly strain-rate dependent due to their fiber-dominant property [20, 23], the multidirectional fiber composites having transverse orientation of fibers (i.e. $+45^\circ$, -45° plies) probably show a considerable matrix-dominant behavior: Harding *et al*. [23] indicated that the modulus of epoxy materials increased significantly with increasing strain-rate. Fig. 4 shows values of E_{flex} for the multidirectional fiber composites measured as described above. At a test rate of 0.5 mm/min (i.e. 0.83×10^{-5} m/s), E_{flex} was 45.1 GPa.

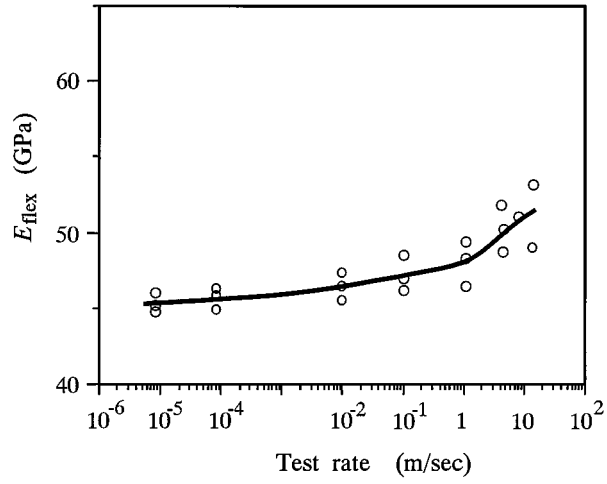

Figure 4 Flexural modulus E_{flex} measured as a function of test rate.

As the rate increased to 1 m/s, E_{flex} reached 47.4 GPa. For the rate beyond 1.0 m/s, values of E_{flex} were considerably scattered but more enlarged on average. At 11.4 m/s, average value of E_{flex} was 51.3 GPa.

An ultrasonic test was conducted to evaluate the dynamic modulus of the multidirectional fiber composite. In this study the "zero order" longitudinal propagation (s_0) of Lamb waves in thin composite plates was measured in a similar way as Blackman *et al*. did [20]. For the longitudinal propagation of Lamb waves in the case where the frequency times thickness product approaches zero, the phase velocity of s_0 tends to the longitudinal velocity of the plate wave (c_0) [24] given by

$$C_0=\left[\frac{E_{11}}{\rho(1-\nu^2)}\right]^{1/2} \tag{14}$$

for plane strain conditions in the plate, where ρ is the specimen density (=1563 kg/m^3) and ν is the Poisson's ratio of the material (=0.29). Though the longitudinal vibration mode in the multidirectional fiber composite plates was observed to propagate with substantial dispersion of the phase velocity, value of velocity in the specimen longitudinal direction measured at 0.6 MHz transmitting frequency was around 6214 m/s. This value of c_0 provided a value of $E_{11}=55.4$ GPa for the ultrasonic axial modulus. Because the ultrasonically measured value was considerably higher than that (51.3 GPa) of the flexural modulus at a test rate of 11.4 m/s, it is expected that the flexural modulus can be still much larger as the test rate increases more.

4. Results and discussion

4.1. Load versus time curves

Load (P) versus time (t) traces of the multidirectional DCB specimens tested at four different rates of test are exhibited in Fig. 5. Several characteristic behaviors can be observed in the traces.

Firstly, at a test rate of 1.0×10^{-2} m/s (Fig. 5a), the load increased showing a linear elastic behavior with an increase of time in advance of the crack initiation, but

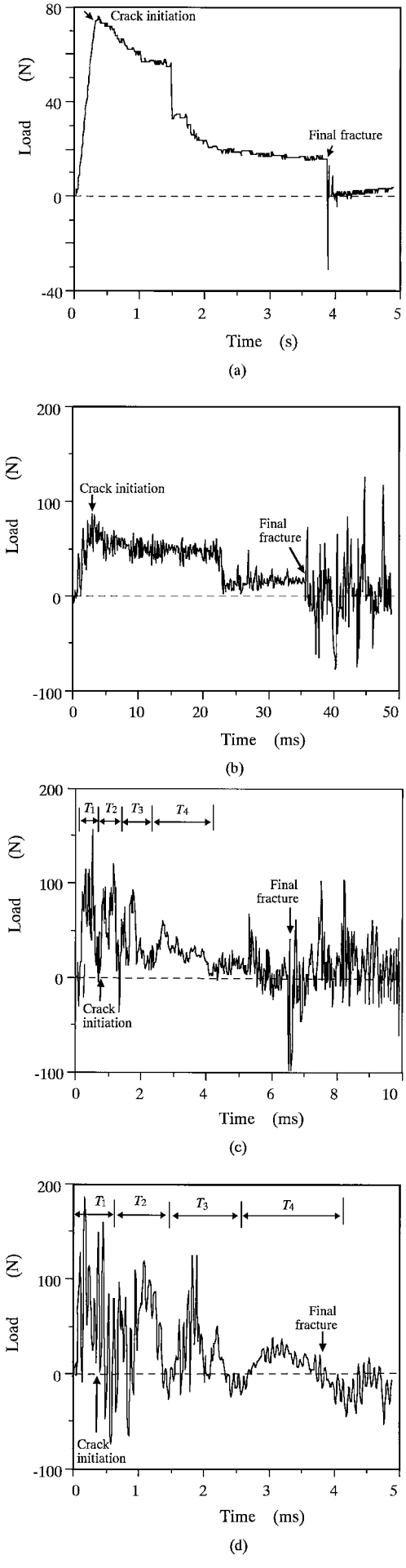

Figure 5 Typical load (P)-time (t) traces of the DCB multidirectional composite specimens under a specimen arm displacement rate of (a) 1.03×10^{-2} m/s, (b) 1.0 m/s, (c) 5.7 m/s and (d) 11.4 m/s.

decreased little by little as the crack began to propagate. During the initial propagation of the crack, fiber bridging might be formed behind the crack tip, hindering the crack propagation and thus, supporting the external load considerably. The stable crack propagation was followed by a sudden and rapid propagation which led to a drastic load-drop in the trace. After crack arrest, the load decreased little by little again due to stable crack propagation.

Secondly, however, Fig. 5b, c and d show dynamic behaviors of increasing the test rate. The presence of many oscillations on the trace arose from the dynamic effects. These dynamic effects are likely to occur from several causes: The first peak in the trace was greatly influenced by inertia effects. The following multiple oscillations were caused by resonant vibration due to a "spring-mass effect" of the specimen and loading rigs, as well as stress waves propagating in the specimen. Resonant frequency f_r may be estimated as 0.6–1.4 kHz through the spring-mass resonance equation [25]

$$f_r = \frac{1}{2\pi} \cdot \left(\frac{K_e}{M}\right)^{1/2} \tag{15}$$

where M is the total mass of the specimen, a lower end-block and a lower loading shackle; K_e is the effective transverse stiffness, i.e., a function of flexural modulus and crack length of the specimen between the upper and lower loading shackles. The "spring-mass effect" appeared clearly in the load-time traces measured at the test rates beyond 3 m/s. The periods of resonance, T_1, T_2, T_3 ..., as shown in Fig. 5c and d, indicated resonant frequencies $f_{1r} \approx 1.4$ kHz, $f_{2r} \approx 1.23$ kHz, $f_{3r} \approx 0.97$ kHz, ... in the interlaminar fracture tests, respectively.

Another possible cause for the oscillations may be the flexural wave propagation in the DCB specimen. Its wave speed C_f, a function of crack length a given [26] by

$$C_f = \left(\frac{35}{74}\right)^{1/2} \cdot \left(\frac{h}{a}\right) \cdot \left[\frac{E_{11}}{\rho(1-\nu^2)}\right]^{1/2} \tag{16}$$

is calculated to be 220 m/s at the initial crack length and, thus, frequency of the wave traveling in the specimen is estimated to be about 3.8 kHz. The frequent oscillations along the load-time trace measured at test rates $\geq$1.0 m/s (as shown in Fig. 5b–d) had frequencies mainly in ranges 3.1–3.8 kHz, which might correspond to the flexural wave reflections. The other cause may be the shear wave propagation having the predicted frequencies of 10–30 kHz. Because the measured frequencies of the load signals were distributed in ranges below 4 kHz without any filtering-out of the oscillations, the oscillations are believed to have come from the "spring-mass effect" and flexural wave propagation.

Thirdly, at test rates $\geq$3 m/s, the crack initiation time point (which was measured with a sequence of high-speed photographic films) (i.e., Fig. 6) was observed around the the first valley site in the load-time trace (see arrow in Fig. 5c and d), which is contradictory to

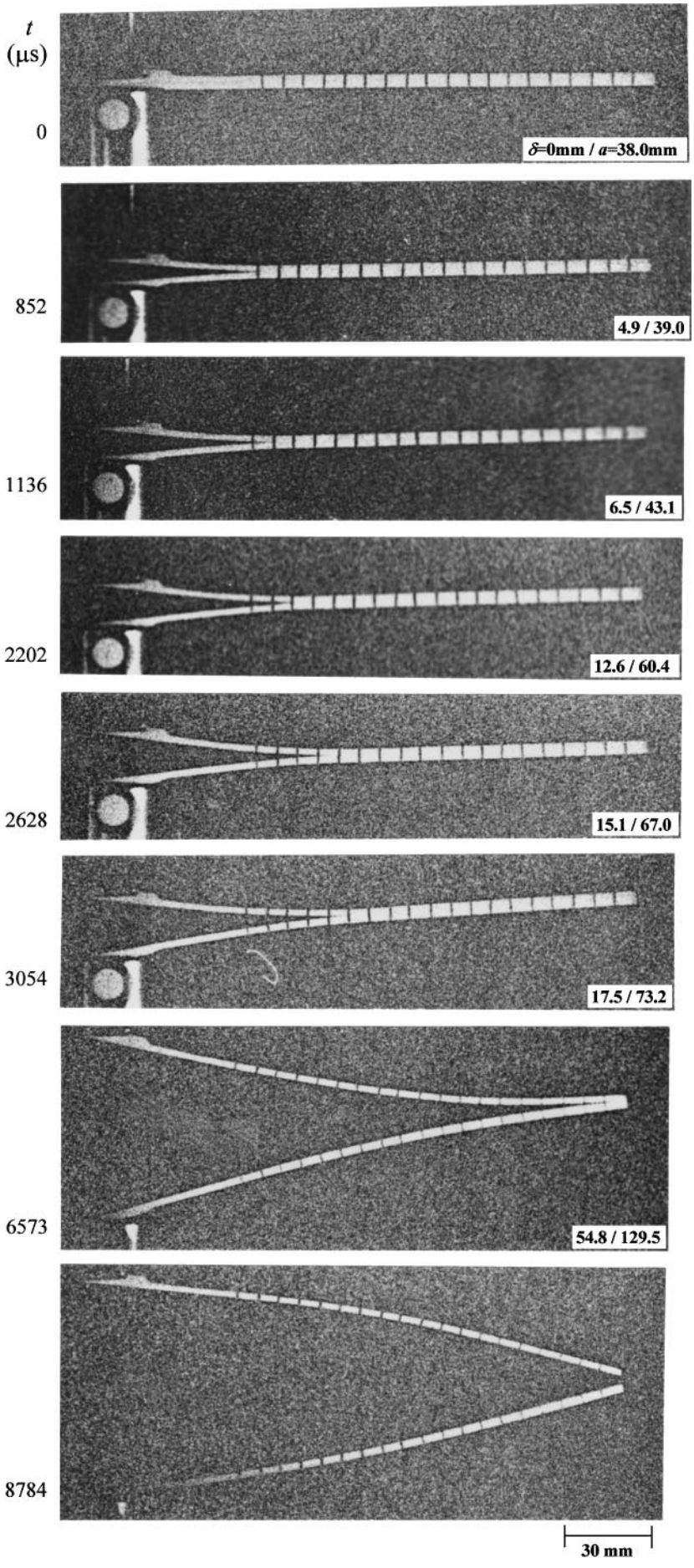

Figure 6 High speed film photographs of a DCB specimen tested at a rate of 5.7 m/s.

the general load-time behavior in the static test where the crack initiation time corresponded to the maximum load point. Therefore, any load values obtained from such traces are very susceptible to errors, since the true load representing the material behavior may be largely obscured by the dynamic effects. For these reasons, Equations 5 and/or 11 can be adopted to enable the fracture energy to be deduced without a knowledge of the applied load.

4.2. Fiber bridging effects on G_{IC} in slow-rate tests

To characterize the mode I delamination fracture of multidirectional fiber $(-45^\circ/0^\circ/+45^\circ)_{2S}$ $(+45^\circ/0^\circ/-45^\circ)_{2S}$ layup composites under high rates of test, studies on the slow-rate test (0.5 mm/min) are very significant because the delamination fracture energy G_{IC} is a strong function of the length of propagating crack due to the large extent of crack jumping and ensuing fiber bridging [15]. Now, from Equation 2, the value of χ_I may be deduced by plotting the measured values of $(C/N)^{1/3}$ versus the corresponding values of the crack length a. An example of such a plot for a multidirectional fiber composite specimen used in this study is shown in Fig. 7. A linear fit is drawn on the basis of the experimental data. The average value of χ_I was 0.47 ± 0.92, which is much lower than that (3.0 ± 0.38 [5, 20]) of the unidirectional fiber/epoxy composite. The low value of χ_I indicates a relatively small rotation and deflection of the crack tip on account of the large scale fiber bridging behind the crack tip.

While the linear fit appears to be reasonable in Fig. 7, some deviation of the individual experimental points from the linear fit indicates that the values of the effective flexural modulus, $E_{c/n}$ and χ_I, do vary considerably during the course of crack propagation as the crack jumps into different neighbouring plies and fiber bridging develops behind the crack tip. The values of $E_{c/n}$ of the specimen beam may be obtained at each

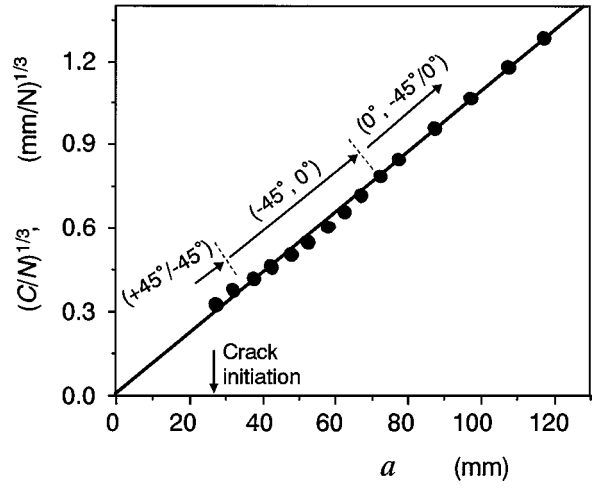

Figure 7 $(C/N)^{1/3}$ versus the propagating crack length a.

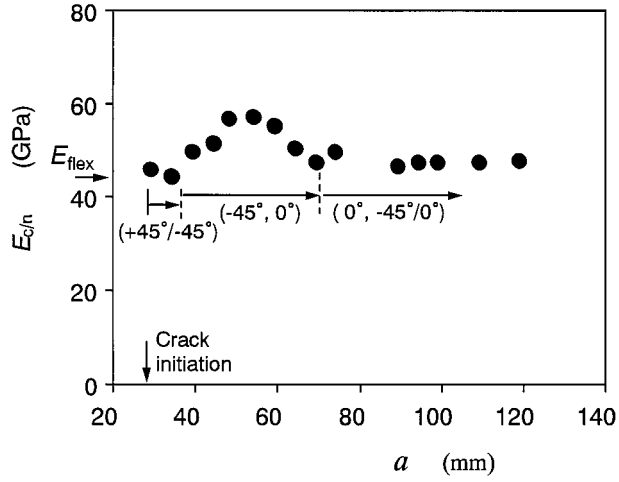

Figure 8 The effective flexural modulus, Ec/n, versus the length a of the propagating crack for the multidirectional laminate, which varied with the crack jumping process. The specimen was the same as that of Fig. 7.

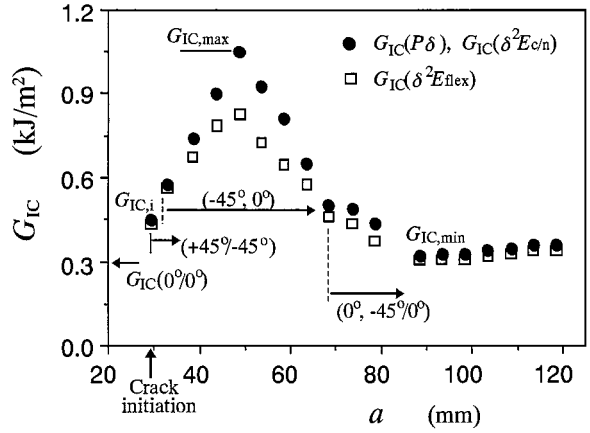

Figure 9 Values of the Mode I interlaminar fracture energy G_{IC}, obtained by the two data reduction schemes, versus the length a of the propagating crack for the multidirectional laminate. The specimen was the same as those of Figs 7 and 8.

propagating crack length a from Equation 3, which is given by

$$E_{c/n} = 8N\frac{(a + \chi_I h)^3}{Bh^3} \cdot \left(\frac{P}{\delta}\right). \qquad (17)$$

Fig. 8 shows typical values of $E_{c/n}$ calculated from the measured compliance as a function of a for the specimen used in Fig. 7. For the very initial stages of crack growth on the $+45^\circ/-45^\circ$ interface, the value of $E_{c/n}$ was almost equal to the independently measured value of the flexural modulus of the composite beam ($E_{flex} \cong 45.1$ GPa). However, as the crack had jumped into adjacent plies (-45°, 0°) and considerable fiber bridging had developed behind the crack tip, the value of $E_{c/n}$ increased to a maximum value ($\cong$57.3 GPa) at $a = 53$ mm. With further crack growth, $E_{c/n}$ decreased to a value of about 47.4 GPa and then fluctuated, in which stage the crack had almost completely moved into the 0° ply and along the $-45^\circ/0^\circ$ interface.

Utilizing Equations 4 and 5, the values of G_{IC} of the specimen in Fig. 7 may be measured as a function of the propagating crack length a, which is presented in Fig. 9.

The results obtained through Equation 4 [denoted by "$G_{IC}(P\delta)$"] are straightforward to deduce. In Equation 5 [denoted by "$G_{IC}(\delta^2\ E)$"], however, the value of the axial modulus E_{11} of the composite is required: the flexural modulus independently measured by a three-point bend test (E_{flex}) or the effective flexural modulus calculated from the measured compliance ($E_{c/n}$). The two methods termed "$G_{IC}(P\delta)$" and "$G_{IC}(\delta^2\ E_{c/n})$" are equivalent via Equation 17 and give the same values of G_{IC}. As shown in Fig. 9, the value of G_{IC} obtained through Equation 4 at the initiation of crack growth, was almost the same in value ($\cong$0.46 kJ/m^2) as that through Equation 5. This is because the value of $E_{c/n}$ at the crack onset was almost similar to E_{flex}, as revealed in Fig. 8. Immediately after the crack began to grow, however, a few intraply (-45°) fractures occurred. This was in addition to the interlaminar ($+45^\circ/-45^\circ$) fractures as observed on the fracture surfaces of the corresponding specimen (Fig. 10a and b), which caused a relatively higher value of G_{IC} at the crack initiation for the present composite (in contrast to that of the unidirectional composite, 0.30 kJ/m^2 [5, 20]). With an increase of a to about 48 mm, a "rising R-curve" became prominent: the maximum value of G_{IC} ($G_{IC,max}$) was obtained from the "$G_{IC}(\delta^2\ E_{flex})$", which was considerably lower, by about 13%, than that from the "$G_{IC}(P\delta)$". This is because the value of E_{flex} was considerably lower than that of $E_{c/n}$ (Fig. 8) caused by the presence of the fiber bridging behind the crack tip. At $a \cong 48$ mm the major part of the crack front jumped into the neighboring plies to produce the intraply ($-45^\circ, 0^\circ$) fractures (Fig. 10a), inducing crack tip splitting and a high degree of fiber bridging behind the crack tip, and thus significantly enlarging the value of $E_{c/n}$. At longer crack lengths, when the crack jumped into the 0° ply, it resulted in an intraply (0°) fracture, which was initially accompanied by a high degree of fiber bridging. Indeed many broken fibers resulted from the fiber-bridging effect were observed on the non-planar, 0°, fracture surface. As the crack steadily propagated via an intraply fracture through the 0° ply, the degree of fiber bridging decreased. The value of G_{IC} eventually decreased to the minimum value ($G_{IC,min}$) of 0.30 kJ/m^2.

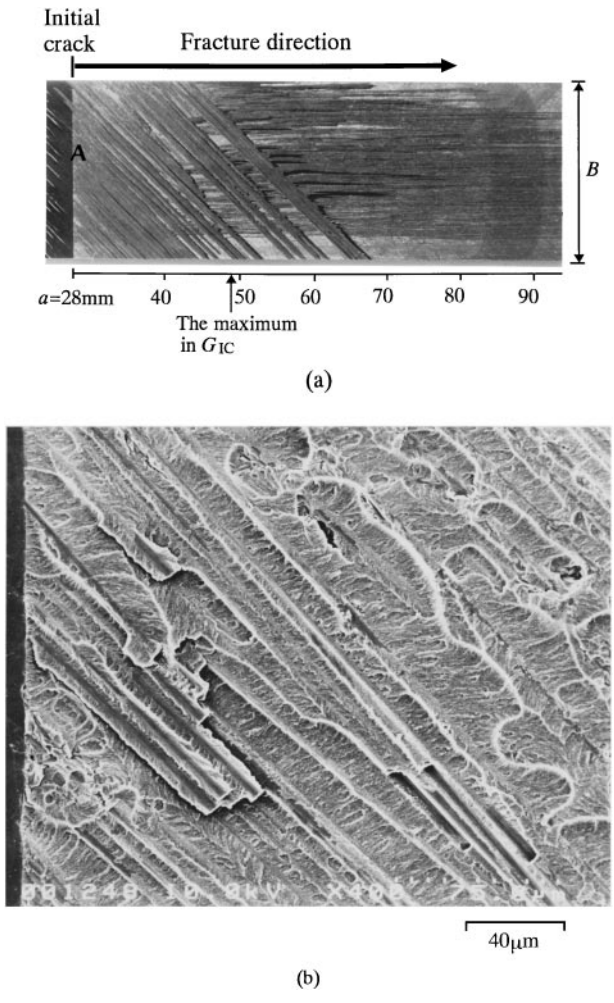

Figure 10 Optical photograph (a) of the fracture surface for the specimen used in Fig. 9 and scanning electron micrograph (b) of region "A", as indicated in (a).

The values of G_{IC}, determined by Equation 4, were usually in excellent agreement with those by the compliance calibration method described in the ASTM Standard Test Method for DCB tests [27]; no difference greater than 5% was ever recorded. Thus, Equation 4, "$G_{IC}(P\delta)$", which does not require a value of the modulus to be used, is suggested as the best method for deducing the values of G_{IC} for the multidirectional fiber composites in the slow-rate tests.

As stated in Section 4.1, however, any load values obtained from load-time traces in the high rates of tests $\geq$1.0 m/s are largely obscured by the dynamic effects and very susceptible to errors. Thus, Equation 5 or 11, not Equation 4, might be better employed for deduction of the value of G_{IC}. Because the value of G_{IC} at the crack initiation ($G_{IC,i}$) and the minimum value ($G_{IC,min}$) obtained via Equation 5 were equivalent to those via Equation 4, Equation 5 or 11 may be used for the deduction of $G_{IC,i}$ and $G_{IC,min}$. However, the values of $G_{IC,max}$ obtained through Equations 5 and 11 can be considerably underestimated (as described in Fig. 9), and thus have to be compensated for the loss, which may be given by

$$G_{IC,max} = 1.15\ G_{IC}(\delta^2 E_{flex}) \tag{18}$$

and

$$G_{IC,max} = 1.15\ G_{IC}\left(\delta^2 E_{flex}\right) - \frac{111 E_{11} h}{1120}\left(\frac{V}{C_l}\right)^2 \tag{19}$$

respectively. Thus, Equation 18 or 19 is suggested as a better method for deducing the maximum values of G_{IC} for the multidirectional fiber composites in the high-rate tests.

4.3. Variation of crack length and crack velocity with time

For the slow rate tests, the crack lengths with time during the test were monitored by visual observation through a travelling microscope. For the high rate tests, on the other hand, crack lengths as well as opening displacements of specimen arms were measured by high-speed film (see Fig. 6) which recorded the progress of the test.

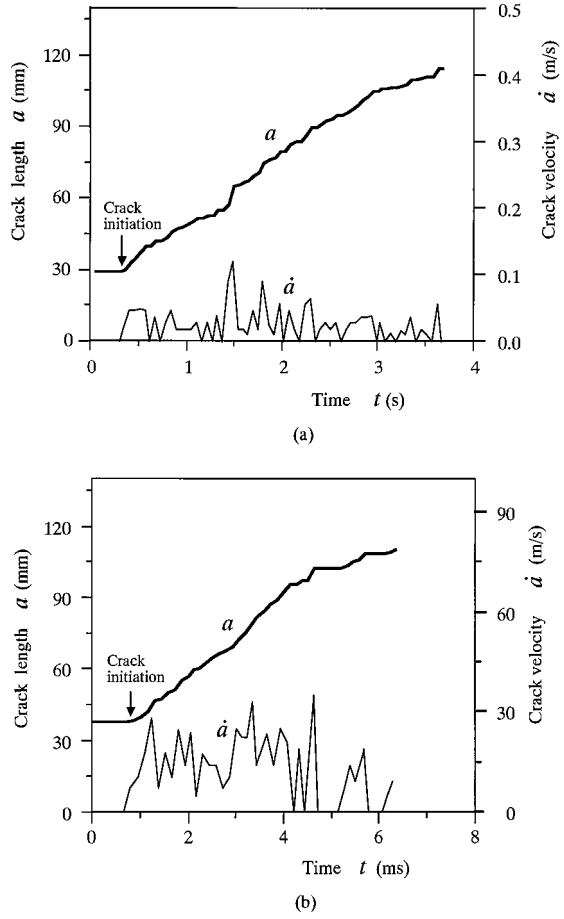

Figure 11 Typical traces of the propagating crack length a and the corresponding crack velocity $\acute{a}$ as a function of time for the DCB specimens tested at a rate of (a) 1.03×10^{-2} m/s and (b) 5.7 m/s.

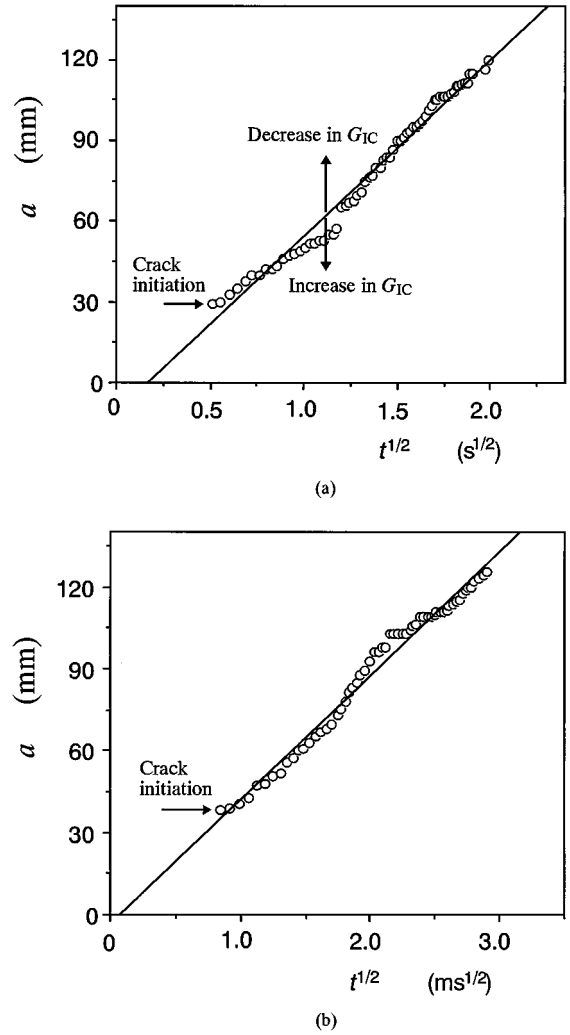

Figure 12 Values of crack length as a function of root time for the same DCB specimens as used in Fig. 11a and b, tested at a displacement rate of (a) 1.03×10^{-2} m/s and (b) 5.7 m/s, respectively.

Fig. 11a shows the variation of the length of the propagating crack a and its corresponding crack velocity $\acute{a}$, with time t for the multidirectional fiber composite specimen in Fig. 5a at a test rate of 1.0×10^{-2} m/s. The variation of $\acute{a}$ with time in this figure reflects the sequence of short periods of "stick-slip" growth of crack i.e., short repetitions of stable and then rapid cracking, which revealed the overall appearance of stable crack growth through the length of the DCB specimen. It is to be noted that the experimentally measured value of $\acute{a}$ could be different according to the framing rate of the camera because the values of $\acute{a}$ were obtained by averaging the two frame data of crack length and the corresponding time in high-speed films. The crack velocity was measured to be of the order of 0.01–0.13 m/s before crack arrest occurred when the velocity was zero. Fig. 11b gives the results obtained at a rate of 5.7 m/s, showing the highly transient behaviors of $\acute{a}$ versus time as the crack propagated through the DCB specimen. The maximum crack velocity was much higher up to 34 m/s than that for the slow rate test, as would be expected for this high test-rate.

When we assume the steady state propagation of crack where the value of G_{IC} is constant, a graph of a versus $t^{1/2}$ should be linear with gradient A as given in Equations 6 and 7. The graphs of a described as a function of t in Fig. 11a and b were transformed into graphs of a versus $t^{1/2}$ shown in Fig. 12a and b, respectively. The linear fits to the propagation data shown in Fig. 12a and b produced gradients A = 65.7 mm $(s)^{-1/2}$ and 45.4 mm $(ms)^{-1/2}$, respectively. However the experimentally recorded values of a showed a large magnitude of oscillations about the straight fitting line predicted by the steady state. The variation of the measured crack length values will directly affect a variation into the deduced values of G_{IC} when either Equation 5 or 11 is employed: Equations 6 and 7 indicate that an increased interlaminar fracture energy G_{IC} at a time during the crack propagation can cause a decrease in A, thus causing a shorter crack length at the corresponding time. It is considered that the irregular variations of the crack velocity and the large magnitude of crack length oscillations occurred not only because of such complicated propagation behavior as crack jumping and fiber bridging, but also because of the dynamic effects described in Section 4.1.

From Equation 6 the crack velocity in the steady state is derived as a function of time t

$$\dot{a} = \frac{A}{2t^{1/2}} \tag{20}$$

and thus, the crack velocity normalized by the specimen arm displacement rate V is given by

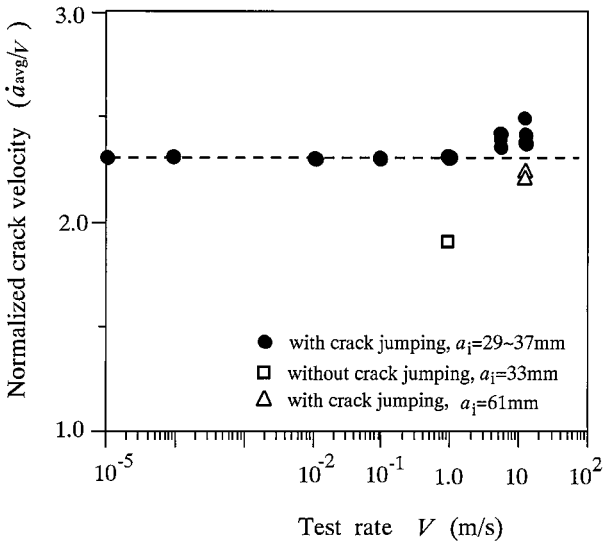

Figure 13 Values of the average crack velocity of the DCB specimens normalized by a test rate ($\dot{a}_{avg}/V$) as a function of the test rate.

$$\dot{a}/V = \frac{1}{2}\left(\frac{3}{16}\frac{F}{N^2}\cdot\frac{h^3E_{11}}{G_{IC}\delta^2}\right)^{1/4} \qquad (21)$$

The average crack velocity $\dot{a}_{avg}$ over the total crack propagation length up to $a = 113$ mm (not showing the edge effect of the specimen end in advance of the final separation point of the DCB specimen) is shown in Fig. 13. Values in this figure are the ones normalized by V ($=\dot{a}_{avg}/V$). It is seen here that, at the slow test rates below 1.0 m/s, values of $\dot{a}_{avg}/V$ were almost equal to a value of 2.3, whereas at the high rates beyond 1.0 m/s those values were considerably larger than 2.3. The presence of the increment in $\dot{a}_{avg}/V$ at the rates $\geq$1.0 m/s is considered to have been affected by the decrease in the average value of G_{IC}, as indicated in Equation 21. However, the case of symbol □ in the figure indicates a drastically lower value. A fracture surface examination for the corresponding specimen exhibited there exposed little crack jumping behavior and suggested that strong fiber bridging being developed behind the crack tip had been kept up to the final separation time, bringing about a significant increase in the average value of G_{IC} over the total crack length therefore, a reduction of $\dot{a}_{avg}/V$. The above results were obtained from the specimens with initial crack lengths of $a_i = 29$–37 mm. However, in the case of $a_i = 61$ mm (symbol Δ), values of $\dot{a}_{avg}/V$ were a bit lower. One reason for the decrease in $\dot{a}_{avg}/V$ may be that the average value of G_{IC} over the total propagation length increased due to the crack jumping and ensuing fiber bridging proceeding through the majority of the crack propagation length. The other reason may be that the deformation rate at the crack tip decreased due to lower bending stiffness of the specimen arms, causing the actual dynamic loading rate at the crack tip to be less than the loading rate for short crack length. Besides, the strong flexural waves caused by the impactive loading were slightly relaxed due to the long distance between the loading points and the crack tip when the initial crack length is long.

4.4. Rate effects on G_{IC}

In the slow-rate tests, a "rising R-curve" described in Section 4.2 was initially pronounced for the multidirectional laminates, where it was clearly due to the crack jumping from its initial location at the $+45^\circ/-45^\circ$ midplane interface into the neighboring plies, thereby giving rise to extensive crack tip splitting and large-scale fiber-bridging. Actually, when the value of G_{IC} is plotted as a function of crack length, a very complex relationship may be observed, reflecting the occurrence of complex delamination paths, which gives scattered values of $G_{IC,max}$.

Values of G_{IC} and the corresponding crack velocity $\dot{a}$ for the specimens of Fig. 11a and b were plotted as a function of the propagating crack length a, as shown in Fig. 14a and b, respectively. The sequence of many "stick-slip" crack growths, as exhibited in crack velocity oscillations, caused oscillations of G_{IC} to occur with increase of the crack length. In the slow-rate of 1.0×10^{-2} m/s (Fig. 14a), values of G_{IC}, obtained via Equation 4 [G_{IC} (Pδ)] at the crack initiation, were almost the same as that of Fig. 9 at a rate of 0.5 mm/min. After that, G_{IC} averagely increased to the maximum value (0.83 kJ/m^2) at $a \cong 56$ mm and then eventually decreased to the minimum value of about 0.30 kJ/m^2. The overall behavior of G_{IC} as a function of a was very similar to that in Fig. 9.

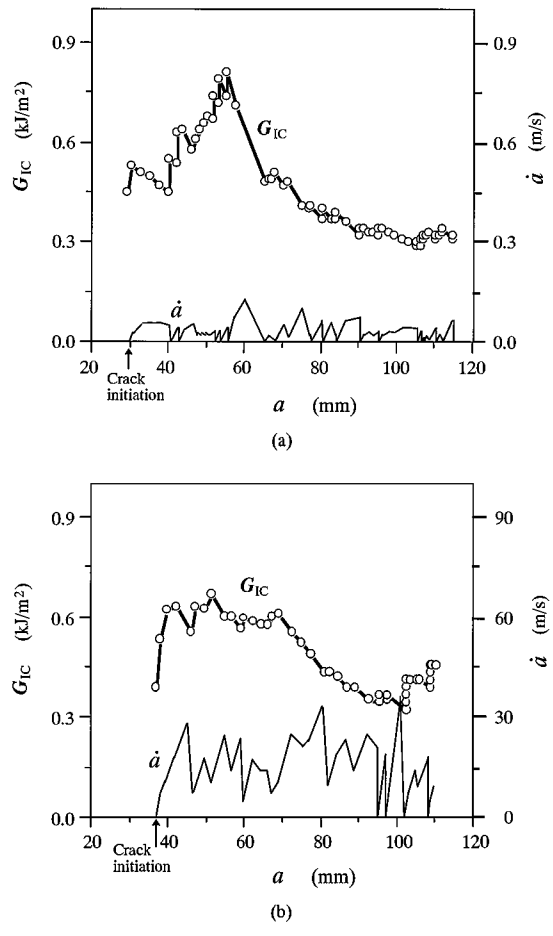

Figure 14 Typical delamination fracture energy G_{IC} and the corresponding crack velocity $\dot{a}$ versus crack length a for the same DCB specimens as used in Fig. 11a and b, tested at a displacement rate of (a) 1.03×10^{-2} m/s and (b) 5.7 m/s, respectively.

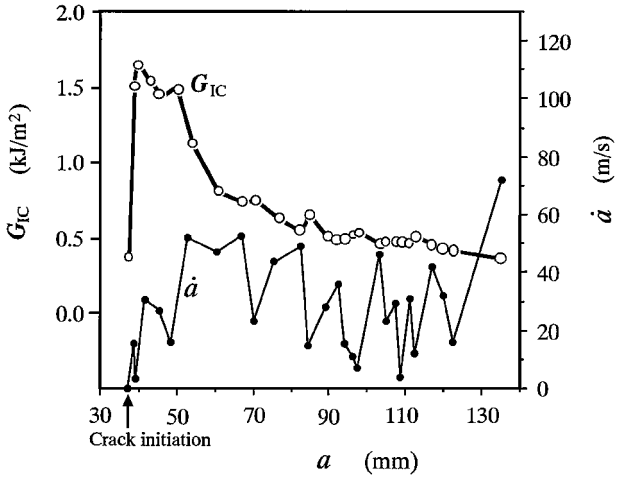

Figure 15 Typical delamination fracture energy G_{IC} and the corresponding crack velocity $\acute{a}$ versus crack length a for a DCB specimen with initial crack length $a_i = 37$ mm, tested at a displacement rate of 11.4 m/s.

Values of G_{IC} for the specimen tested at a rate of 5.7 m/s are shown in Fig. 14b, which were obtained via Equation 11 [G_{IC} ($\delta^2 E_{11}$)]. In comparison with the corresponding value in the slow rate test (Fig. 14a), the value of G_{IC} (0.38 kJ/m^2) at the crack initiation was a bit lower. In the case of $G_{IC,max}$, the value was corrected via Equation 19 to be 0.77 kJ/m^2, which was also lower. However, the minimum value ($\approx$0.30 kJ/m^2) was similar.

Fig. 15 shows a typical feature of G_{IC} values and the corresponding $\acute{a}$ values measured at a rate of 11.4 m/s for the specimen with the initial crack length of $a_i = 37$ mm. The G_{IC} values were obtained via Equation 11. A drastic increase of G_{IC} from $G_{IC,i} = 0.38$ kJ/m^2 to $G_{IC,max} = 1.6$ kJ/m^2 took place during the initial stage of the crack propagation. The corresponding fracture surface is exhibited in Fig. 16. During the initial crack advance of about 3–5 mm, one part of the initial fracture region was still on the $+45^\circ/-45^\circ$ interface (see region D in Fig. 16b, magnified by a scanning electron microscope in the region B of Fig. 16a), while the other part was in the $+45^\circ$ intraply where numerous broken fibers, as well as the complicated non-planar fracture surface, were observed (see region C in Fig. 13a and b). Such severe non-planar fractures in the initial crack growth process was never seen on the fracture surface of specimens tested at rates $\leq$5.7 m/s. This indicates that such an initial stage of cracking was accompanied by a very high degree of fiber bridging; thus, the value of $G_{IC,max}$ obtained at a rate of 11.4 m/s was much larger than that at 5.7 m/s. One reason for the complicated fracture just after the crack initiation may be that the strong flexural waves generated by the impactive loading with a high rate of 11.4 m/s caused the neighboring plies around the crack tip to be damaged just in advance of the crack initiation, rendering the crack tip to significantly split into the neighboring plies and then fiber-bridged during the initial crack growth process. The crack then grew by about 10 mm at a relatively low speed, keeping a high value of $G_{IC} \geq 1.4$ kJ/m^2 (Fig. 15). After that, the crack propagated by about 25 mm with high velocity,

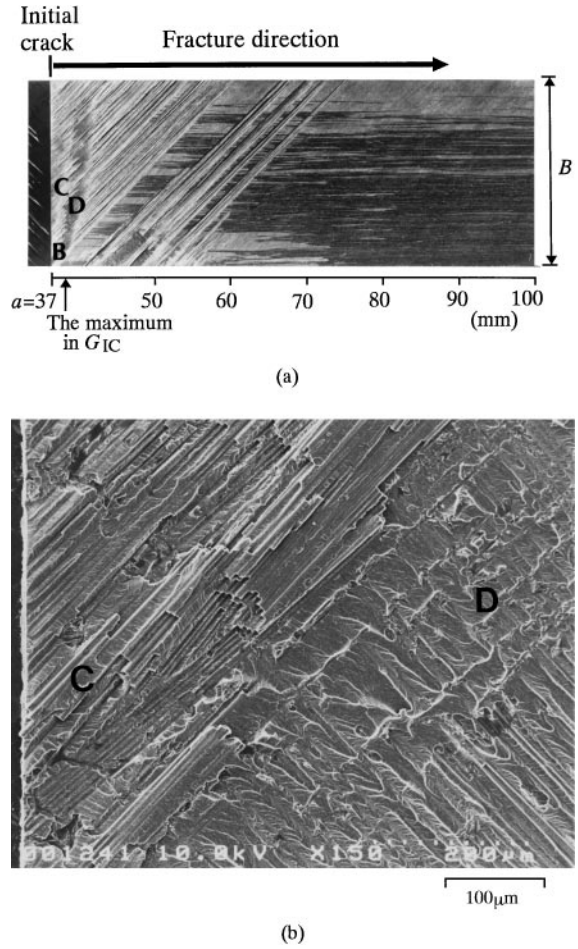

Figure 16 Optical photograph (a) of the fracture surface for the specimen used in Fig. 15 and scanning electron micrograph (b) of region "B" as indicated in (a).

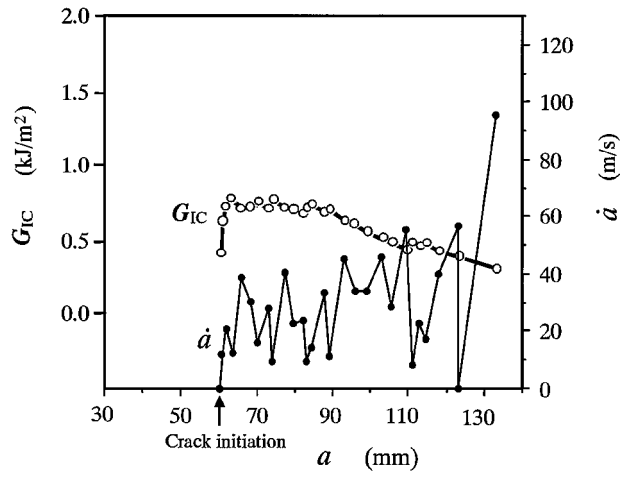

Figure 17 Typical delamination fracture energy G_{IC} and the corresponding crack velocity $\acute{a}$ versus crack length a for a DCB specimen with initial crack length $a_i = 61$ mm, tested at a displacement rate of 11.4 m/s.

giving a drastic decrease in G_{IC}. After several times of "stick-slip" propagation up to $a = 120$ mm, the value of $G_{IC,min}$ was obtained to be about 0.41 kJ/m^2.

The feature of G_{IC} values obtained for the specimen with a long initial crack length of $a_i = 61$ mm is exhibited in Fig. 17. As compared with the case of the specimen with $a_i = 37$ mm (Figs 15 and 16), the values of $G_{IC,max}$ (0.75 kJ/m^2) obtained around $a = 64$–73 mm,

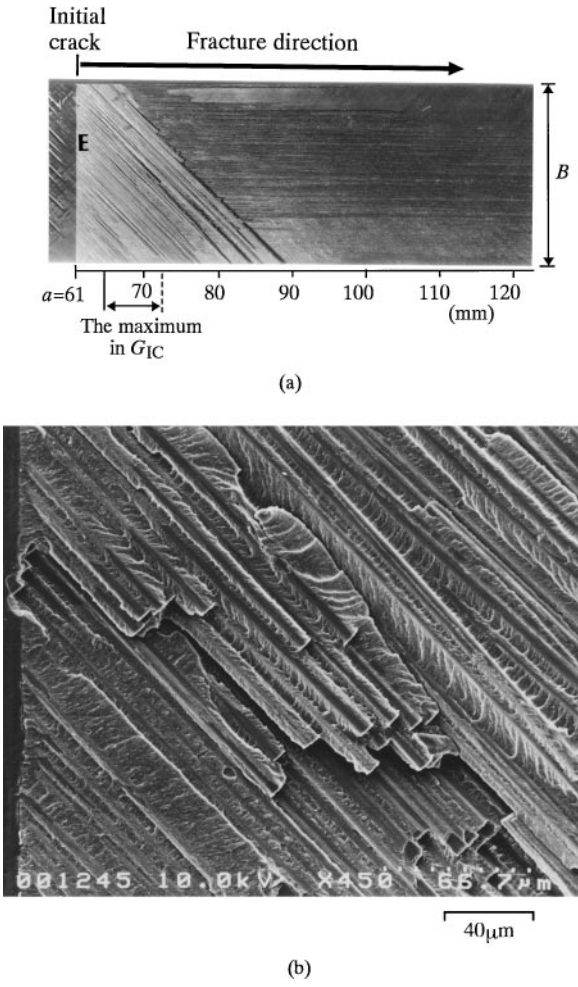

Figure 18 Optical photograph (a) of the fracture surface for the specimen used in Fig. 17 and scanning electron micrograph (b) of region "E" as indicated in (a).

were much lower. In the initial stage of crack propagation the fracture surface (see region E in Fig. 18a and the crack initiation site in Fig. 18b) appeared quite smooth and planar. The crack started to grow on the $+45^\circ/-45^\circ$ plies interface at the mid-plane of the specimen and then shifted only a bit into the adjacent -45° ply, inducing a limited amount of fiber bridging. The amount of broken fibers on the corresponding fracture surface was much less than that of Fig. 16, which explains the low value of $G_{IC,max}$. The long a_i, i.e. long arms of the DCB specimen is considered to have damped the impactive flexural wave oscillations during the propagation of waves through the arm toward the initial crack tip: thus, the high-rate loading with weak flexural wave effects is considered to have been applied to the crack-tip region of the DCB specimen and, resultantly, the flatness of the initial fracture region was obtained similar to the result of the slow-rate test (Fig. 10).

For the multidirectional carbon-fiber/epoxy composites, Fig. 19 summarizes the values of G_{IC} at crack initiation ($G_{IC,i}$), the maximum values ($G_{IC,max}$) and the minimum values ($G_{IC,min}$) as a function of test rate from 0.83×10^{-5} m/s to 11.4 m/s. The values of $G_{IC,max}$ at the high rates $\geq$1.0 m/s were obtained through Equation 19 with compensation for the calculation loss. Several remarks emerge from this figure.

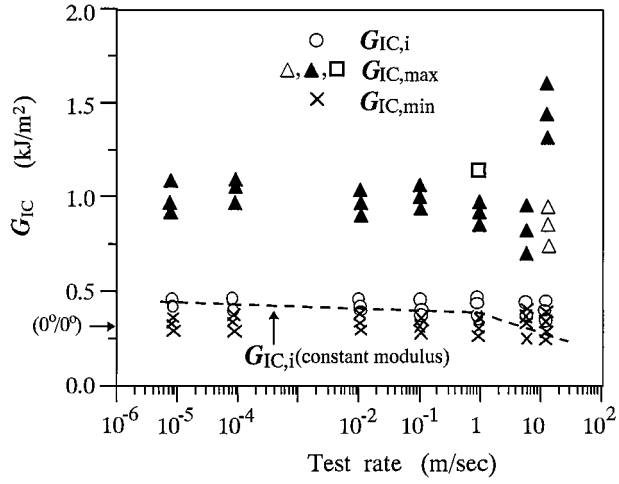

Figure 19 Values of G_{IC} versus displacement rate for the $(-45^\circ/0^\circ/+45^\circ)_{2S}(+45^\circ/0^\circ/-45^\circ)_{2S}$ multidirectional carbon fiber/epoxy composite specimens.

Firstly, there is no major difference in the values for either $G_{IC,i}$, $G_{IC,max}$, or $G_{IC,min}$ with increasing rates up to 1.0×10^{-1} m/s.

Secondly, average values of either $G_{IC,i}$ or $G_{IC,min}$ remained constant with an increase of rate until 1.0×10^{-1} m/s and showed a modest reduction only at rates in excess of 1.0 m/s. This is different from the result of $G_{IC,i}$ (dotted line) obtained without compensation of the axial modulus change with test rates, in which $G_{IC,i}$ decreased gradually with an increase of the test rate from the slow to high rates.

Thirdly, the values of $G_{IC,max}$ decreased considerably with an increase of the rate to 5.7 m/s. At 11.4 m/s, however, $G_{IC,max}$ showed a drastic change depending on the initial crack length a_i : at short a_i, values of $G_{IC,max}$ largely increased while at long a_i they decreased equivalent to the value at 5.7 m/s. The symbol □ mark at a rate of 1.0 m/s represented the specimen with little crack jumping behavior (Fig. 13) where strong fiber bridging had been kept up to the final fracture, inducing a high value of $G_{IC,max}$.

Finally, values of $G_{IC,i}$ at each test rate were a bit larger than those of $G_{IC,min}$. This indicates that the fracture energy at the crack initiation measured along the $+45^\circ/-45^\circ$ plies interface was higher than that obtained during the crack propagation along the $0^\circ/-45^\circ$ plies interface. Values of $G_{IC,min}$ were equivalent to those in the unidirectional fiber/epoxy laminate [5, 20].

5. Conclusions

The present study has shown the experimental results for characterization of the mode I delamination fracture of continuous carbon fiber/epoxy multidirectional composites under a wide range of test rates up to high rates of 11.4 m/s

(1) At the slow rates of test $\leq 1.0 \times 10^{-1}$ m/s the delamination fracture energy showed a "rising R-curve", a strong function of the length of propagating crack due to the large extent of crack jumping and ensuing fiber bridging. In this respect, Equation 4, requiring the

values of the load and displacement, was better for deduction of the interlaminar fracture energy G_{IC} .

(2) At the high rates of test $\geq$1.0 m/s any loads recorded by the load cell were largely obscured by such dynamic effects as "spring-mass" oscillations and flexural wave reflections. In this respect, Equation 11, requiring the values of the actual arm displacement and flexural (axial) modulus, was better for deduction of G_{IC}. However, the maximum value of G_{IC} obtained through Equation 11 was considerably underestimated.

(3) For deduction of G_{IC} via Equation 11, the values of the flexural modulus were determined through the static and dynamic three-point bend test: With an increase of the test rate from 0.5 mm/min to 11.4 m/s, the values of flexural modulus increased from 45.1 GPa to 51.3 GPa. Ultrasonic tests showed that the ultrasonic axial modulus was 55.4 GPa and, thus, the dynamic modulus could be much larger with a further increase of the rate.

(4) At the high rates of test $\geq$1.0 m/s, the sequence of short period of "stick-slip" growth of cracking was exhibited, reflecting highly transient behaviors of crack velocity as the crack propagated through the specimen. The crack velocity normalized by the displacement rate was significantly influenced by the initial crack length, as well as the average value of G_{IC} over the total crack propagation length.

(5) With an increase of the rate up to 1.0×10^{-1} m/s, there was little difference in the delamination fracture behaviors. However, with an increase of the rate beyond 1.0 m/s, the maximum values of G_{IC} decreased considerably. In the case of short initial crack length, however, the maximum values largely increased at a rate of 11.4 m/s.

Acknowledgements

The author would like to thank Professors A. J. Kinloch and J. G. Williams of Imperial College of Science, Technology and Medicine for their helpful discussions for this study.

References

1. D. L. HUNSTON, R. J. MOULTON, N. J. JOHNSTON and W. D. BASCOM, in "Matrix effects in Composite Delamination: Mode I Fracture Aspects," Toughened Composites, edited by N. L. Johnston, ASTM STP 937 (1987) p. 74.
2. W. L. BRADLEY, "Relationship of Matrix Toughness to Interlaminar Fracture Toughness," Application of Fracture Mechanics to Composite Materials, edited by K. Friedrich, Composite Materials Series Vol. 6 (Elsevier Science Publishers, 1989) p. 159.
3. X. N. HUANG and D. HULL, *Comp. Sci. Tech.* **35** (1989) 283.
4. P. DAVIES, C. MOULIN, H. H. KAUSCH and M. FISCHER, *ibid.* **39** (1990) 193.
5. S. HASHEMI, A. J. KINLOCH and J. G. WILLIAMS, *Proc Royal Soc. London* **A427** (1990) 173.
6. *Idem., J. Comp. Mater.* **24** (1990) 918.
7. J. G. WILLIAMS, *ibid.* **21** (1987) 330.
8. L. A. CARLSSON and J. W. GILLESPIE, JR, "Mode II Interlaminar Fracture of Composites," Application of Fracture Mechanics to Composite Materials, edited by K. Friedrich, Composite Materials Series Vol. 6 (Elsevier Science Publishers, 1989) p. 113.
9. Y. WANG and J. G. WILLIAMS, *Comp. Sci. Tech.* **43** (1992) 251.
10. C. CORLETO and W. L. BRADLEY, "Mixed Mode Fracture in Fibre-Polymer Composite Laminates," Composite Materials: Fatigue and Fracture, edited by T. K. O'Brien, ASTM STP1110 (1991) p. 143.
11. J. J. PLOAHA, B. D. DAVIDSON, R. C. HUDSON and A. PIERACCI, *J. Reinf. Plastics Comp.* **15** (1996) 141.
12. D. J. NICHOLLS and J. P. GALLAGHER, *ibid.* **2** (1983) 2.
13. H. CHAI, *Composites* **15** (1984) 277.
14. P. ROBINSON and D. Q. SONG, *J. Comp. Mater.* **26** (1992) 1554.
15. N. S. CHOI, A. J. KINLOCH and J. G. WILLIAMS, *ibid.* **33** (1999) 73.
16. A. J. SMILEY and R. B. PIPES, *ibid.* **21** (1987) 670.
17. PH. BEGUELIN, M. BARBEZAT and H. H. KAUSCH, *Journal de Physique III France* **1** (1991) 1867.
18. G. YANIV and I. M. DANIEL, "Hight-Tapered Double Cantelever Beam Specimen for Study of Rate Effects on Fracture Toughness of Composites," Composite Materials: Testing and Design ASTM STP972, edited by J. D. Whitcomb, Philadelphia (1988) p. 241.
19. A. A. ALIYU and I. M. DANIEL, "Effects of Strain Rate on Delamination Fracture Toughness of Graphite/Epoxy," Delamination and Bonding of Materials, ASTM STP876, edited by W. S. Johnson, Philadelphia (1985) p. 336.
20. B. R. K. BLACKMAN, J. P. DEAR, A. J. KINLOCH, H. MACGILLIVRAY, Y. WANG, J. G. WILLIAMS and P. YAYLA, *J. Mater. Sci.* **30** (1995) 5885.
21. B. R. K. BLACKMAN, A. J. KINLOCH, Y. WANG and J. G. WILLIAMS, *ibid.* **30** (1996) 4451.
22. L. YONGNING, Z. JINGHAU and Z. HUIJUI, *Eng. Frac. Mech.* **39** (1991) 955.
23. J. HARDING, "The Effect of High Strain Rate on Material Properties," in Materials at High Strain Rates, edited by T. Z. Blazynski (Elsevier Applied Science, London, 1987) p. 133.
24. H. KOLSKY, "Stress Waves in Solids" (Constable Dover Publications, New York, USA, 1963).
25. J. G. WILLIAMS, "Fracture Mechanics of Polymers" (Ellis Horwood Ltd, Chichester, UK, 1987) p. 237.
26. Y. WANG and J. G. WILLIAMS, *Composites* **25** (1994) 323.
27. ASTM, "Standard Test Method for Mode I Interlaminar Fracture Toughness of Unidirectional Fiber-Reinforced Polymer Matrix Composites," D5528-94a (1994).

Received 14 March
and accepted 19 October 2000